IOP Publishing Journal of Physics D: Applied Physics

J. Phys. D: Appl. Phys. **49** (2016) 084002 (10pp) doi:10.1088/0022-3727/49/8/084002

Innovative molecular-based fluorescent nanoparticles for multicolor single particle tracking in cells

Jonathan Daniel[1,2], Antoine G Godin[3,4], Matthieu Palayret[3,4], Brahim Lounis[3,4], Laurent Cognet[3,4] and Mireille Blanchard-Desce[1,2]

[1] University of Bordeaux, ISM, UMR 5255, 33 405 Talence, France
[2] CNRS, ISM, UMR 5255, 33 405 Talence, France
[3] University of Bordeaux, LP2N, UMR 5298, 33400 Talence, France
[4] Institut d'Optique & CNRS, LP2N, UMR 5298, 33400 Talence, France

E-mail: mireille.blanchard-desce@u-bordeaux.fr and laurent.cognet@u-bordeaux.fr

Received 4 August 2015, revised 23 November 2015
Accepted for publication 2 December 2015
Published 20 January 2016

Abstract

Based on an original molecular-based design, we present bright and photostable fluorescent organic nanoparticles (FONs) showing excellent colloidal stability in various aqueous environments. Complementary near-infrared emitting and green emitting FONs were prepared using a simple, fast and robust protocol. Both types of FONs could be simultaneously imaged at the single-particle level in solution as well as in biological environments using a monochromatic excitation and a dual-color fluorescence microscope. No evidence of acute cytotoxicity was found upon incubation of live cells with mixed solutions of FONs, and both types of nanoparticles were found internalized in the cells where their motion could be simultaneously tracked at video-rate up to minutes. These fluorescent organic nanoparticles open a novel non-toxic alternative to existing nanoparticles for imaging biological structures, compatible with live-cell experiments and specially fitted for multicolor single particle tracking.

Keywords: nanoparticles, fluorescence, multicolor imaging, single particle tracking, quadrupolar dyes, brightness

S Online supplementary data available from stacks.iop.org/JPhysD/49/084002/mmedia

(Some figures may appear in colour only in the online journal)

1. Introduction

The study of complex biological processes often requires the simultaneous observation of several proteins in live cells. Over the past decade, fluorescence multicolor imaging, and more recently multicolor single-molecule microscopy, has become the tool of choice to investigate the function of biological systems. This requires that, at least, two spectrally-separated emitters can be simultaneously detected. In that context, organic emitting dyes (i.e. fluorophores) have been widely used in fluorescence microscopy because of their high spectral diversity, their compatibility with many imaging techniques, their structural versatility and their ability for bioconjugation. However, molecular fluorophores usually suffer from limited brightness and reduced photostability, which sets limitations for their use in single particle tracking (SPT) experiments for direct observation of molecular interactions between single molecules. To this aim, various series of organic dyes have been optimized in recent years, such as the Alexa and Atto dyes [1, 2], which are typically derived from cyanine or rhodamine molecular schemes. These dyes show rather small Stokes' shifts which is not ideal for simultaneous multicolor microscopy.

Various strategies have been developed in order to overcome the limitations of conventional organic dyes in terms

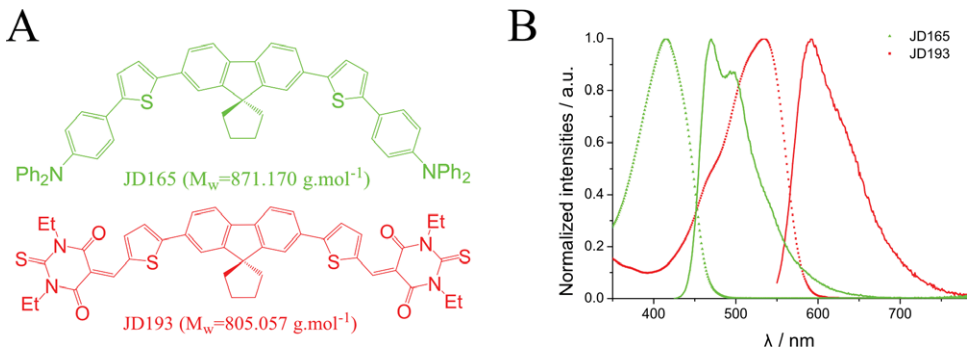

Figure 1. Molecular formulae of JD165 and JD193 dyes (A); and their absorption and emission spectra in chloroform (B).

of brightness and photostability in water. For example, fluorescent proteins [3, 4] or dendrimers [5] were designed with multiple chromophores immobilized within an organic architecture such that the emitters are shielded from the aqueous environment. Another approach is based on fluorescent organic nanoparticles (FONs) where dye subunits are closely packed into confined regions within solid-like nanoparticles (or nanocrystals) [6, 7]. Such molecular-based nanoparticles are easily obtained by nano-reprecipitation of dedicated insoluble dyes in water [8]. They are a promising alternative to heavy-metal containing quantum dots which display high brightness and remarkable photostability [9, 10] but suffer from intrinsic cytotoxicity (due to their heavy-metal content) and lack of biodegradability (critical for medical applications). Earlier work has shown that dipolar dyes could be chemically engineered to form FONs that combine near-infrared (NIR) emission, high brightness and remarkable colloidal stability (including in cellular environments), high two-photon absorption as well as improved photostability as compared to isolated dyes [11]. Following this strategy, we describe here a set of novel FONs based on a common quadrupolar molecular scheme. Chemically varying the external design encompassing this quadrupolar core, we obtained two FONs emitting in spectrally-separated regions of the spectrum (green versus NIR emission) and characterized by large Stokes' shifts (over 5000 cm^{-1}), a size-dependent brightness (typically about 10^6 M^{-1} cm^{-1} for NIR-emitting nanoparticle of ~15 nm diameter) as well as a good colloidal stability and enhanced photostability compared to conventional dyes. Owing to their large Stokes' shifts, we were able to detect simultaneously green and NIR-emitting FONs at the single particle level using a monochromatic excitation. We also provide evidences of single particle tracking of these FONs as they were internalized in living fibroblast-like COS7 cells.

2. Results and discussion

2.1. Design and photophysical properties of dyes in solution

Two different dyes were synthesized as subunits for the preparation of FONs (figure 1 and supplementary synthesis section (stacks.iop.org/JPhysD/49/084002/mmedia)). These dyes are symmetrical molecules built from a common spirofluorene core and bear either electron-withdrawing (JD193) or electron-releasing end-groups (JD165). Such quadrupolar-type dyes show a low-energy transition characterized by a concerted intramolecular charge transfer (ICT) from the core to the periphery (JD193) or conversely from the periphery to the core (JD165) upon excitation [12]. This feature ensures large transition dipole, similar or larger than for ICT dipolar dyes, without generating large ground-state dipole moments. This is of interest as dipole-dipole interactions promote antiparallel stacking when dipolar dyes are put into close confinement (such as in aggregates and in the solid state), which is strongly detrimental to their fluorescence as the transition from the lower excited-state to the ground state of such dimeric configuration becomes symmetry forbidden. Hence quadrupolar-type dyes offer a promising route towards ultra-bright FONs [13]. In addition, depending on the nature of the end-groups and on the amount of ICT, the photoluminescence properties of quadrupolar dyes may strongly depend on the polarity of their environment as a result of symmetry breaking in the excited state [14–16].

JD165 dye was found to strongly absorb in the blue visible region while JD193 absorbs in the green visible region (figure 1(B)). JD165 shows bright blue-green emission depending on the polarity of the environment while JD193 shows much weaker emission that shifts from yellow in apolar solvents to orange-red in polar solvents (table 1). The much lower fluorescence quantum yield of compound JD193 as compared to JD165 can be ascribed to both smaller radiative decay rate (in relation with red-shifted emission) [17] and larger non-radiative decay rate. This larger non-radiative rate can most probably be ascribed to different processes including internal conversion (vibrational deactivation), intramolecular electron transfer and intersystem crossing. Indeed both dyes show singlet oxygen generation in toluene solution with a much larger quantum yield value for compound JD193 as shown in table 1. This suggests efficient triplet formation for JD193 dye upon excitation.

2.2. Green- and NIR-emitting FONs preparation and characterization

The green and the NIR FONs were prepared by instant addition of a small volume of a stock solution of the dye in tetrahydrofuran (THF) (1.0 mM for JD165 or 0.5 mM for JD193) into a large volume of deionized water. In order to avoid potential

Table 1. Photophysical properties of JD165 and JD193 dyes dissolved in solvents of various polarities, or aggregated within nanoparticles in water.

Cpd/solvent	λ_{abs}^{max} (nm)	ε^{max} (M^{-1} cm^{-1})	$FWHM_{abs}$ [a] (cm^{-1})	λ_{em}^{max} (nm)	$FWHM_{em}$ [b] (cm^{-1})	Stokes'shift (cm^{-1})	Φ_f [c]	Φ_Δ [d]
JD165/Toluene	414	—	4400	462	2600	2510	0.66[e]	0.25
JD165/AcOEt	410	—	4600	464	3500	2840	0.74[e]	
JD165/THF	415	$9.0\ 10^4$	4300	468	3300	2730	0.69[e]	
JD165/$CHCl_3$	415	—	4416	470	2930	2820	—	
JD165/DCM	414	—	4500	474	3500	3060	0.71[e]	
JD165/Acetone	412	—	4300	491	3800	3900	0.76[e]	
JD165/DMF	417	—	4400	501	3900	4020	0.73[e]	
JD165/DMSO	420	—	4400	509	3900	4160	0.70[e]	
JD165 $\subset$ FONs/H_20	400	$5.5\ 10^4$	5300	507	2800	5280	0.14[e]	
JD193/Toluene	527	—	3700	567	2000	1340	0.02[f]	0.50
JD193/$CHCl_3$	534	$1.1\ 10^5$	3400	592	2200	1830	0.03[f]	
JD193/THF	523	$1.1\ 10^5$	3400	585	2300	2030	0.03[f]	
JD193/DCM	530	—	3400	595	2300	2060	—	
JD193/DMF	515	—	3800	628	3400	3490	0.02[f]	
JD193 $\subset$ FONs/H_20	503	$5.5\ 10^4$	5600	716	2900	5910	0.01[f]	

[a] Full width at half maximum of the low-energy absorption band.
[b] Full width at half maximum of the emission band.
[c] Fluorescence quantum yield determined using fluorescein[e] or cresyl violet[f] as standards.
[d] Singlet oxygen generation quantum yield determined using TPP in toluene as standard ($\Phi_\Delta = 0.7$).

toxic effect of the organic solvent, we set the final amount of THF in the FONs suspension to be lower than 1% in volume. After mixing, the liquid instantaneously turned from a colorless to a limpid yellow (JD165) or dark-red (JD193) solution (figure 2(A)). The size of the FONs were estimated using dynamic light scattering (DLS) experiments giving effective hydrated diameters of 103 nm and 52 nm for FONs made from JD165 and JD193 respectively. Transmission electronic microscopy (TEM) confirmed the formation of spherical nanoaggregates with dry diameters of 43 nm and 14 nm, respectively (figure 2(B)). The significant difference between average diameters values derived from TEM and DLS characterization suggests the presence of a shell of solvent molecules tightly bound to the surface of the FONs. This interpretation is supported by the FONs zeta potentials which were found to be highly negative (table 2), with uncommon values ranging from −70 mV (JD165) to −88 mV (JD193). These large values might be responsible for strong interactions between solvent molecules and the FONs surfaces, in particular H-bonds with surrounding water molecules.

Taking into account the size (as determined from TEM, see figures 2(C) and (D) of the nanoparticle, the average number of dye subunits was estimated (see table 2) assuming a mean density of 1 (relative to water). We note that ultra-small JD193 FONs (about three times smaller than JD165 FONs) are composed of ~1000 dye subunits.

2.3. Green- and NIR-emitting FONs optical properties. Effect of molecular confinement

JD165 FONs strongly absorb in the violet-blue region and emit in the green region while JD193 FONs absorb in the whole blue to yellow visible region and emit in the red-NIR region (figure 1(B)). Confinement of the dye subunits within FONs leads to the modification of both absorption and emission spectra as illustrated in figures 3(A) and (B). In both cases, the lower energy absorption band is significantly broadened and its maximum is slightly blue-shifted. In addition, a marked hypochromic shift is observed. This shift is slightly more pronounced in the case of JD193 FONs (i.e. 50%) than for JD165 FONs (i.e. 40%). The formers also show an important red-tail in the low-energy absorption band. This behavior is indicative of interchromophoric interactions between dye subunits favored by molecular confinement. The modification of the absorption spectra points to an excitonic coupling giving rise to excited-state splitting [18]. This is consistent with the observed broadening of the absorption band which can be ascribed to the onset of two sub-bands; a blue-shifted sub-band ('H-type') and a red-shifted sub-band ('J-type') which is more clearly seen in the case of JD193. The relative intensity of both sub-bands depends on the relative orientation of dyes within FONs while the splitting depends on the strength of the excitonic coupling (hence on both the distance between subunits and on the transition dipoles of the dyes) [18]. The more pronounced hypochromic effect and broadening of the absorption band observed for JD193 FONs indicate a stronger excitonic coupling and most probably different relative orientation of dyes within FONs (closer to J-type in the case of dye JD193 and H-type in the case of JD165).

The emission of JD165 and JD193 dyes are also affected upon molecular confinement within FONs. While JD165 FONs show a well-structured emission band whose position is similar to that of JD165 dye dissolved in a polar solvent like DMSO, JD193 FONs show a definite red-shifted emission band as compared to that of JD193 dissolved in polar solvents (see table 1). This behavior is consistent with fluorescence originating from the lowest-energy excited state originating from excitonic splitting. As a result, whereas JD193 is a yellow to

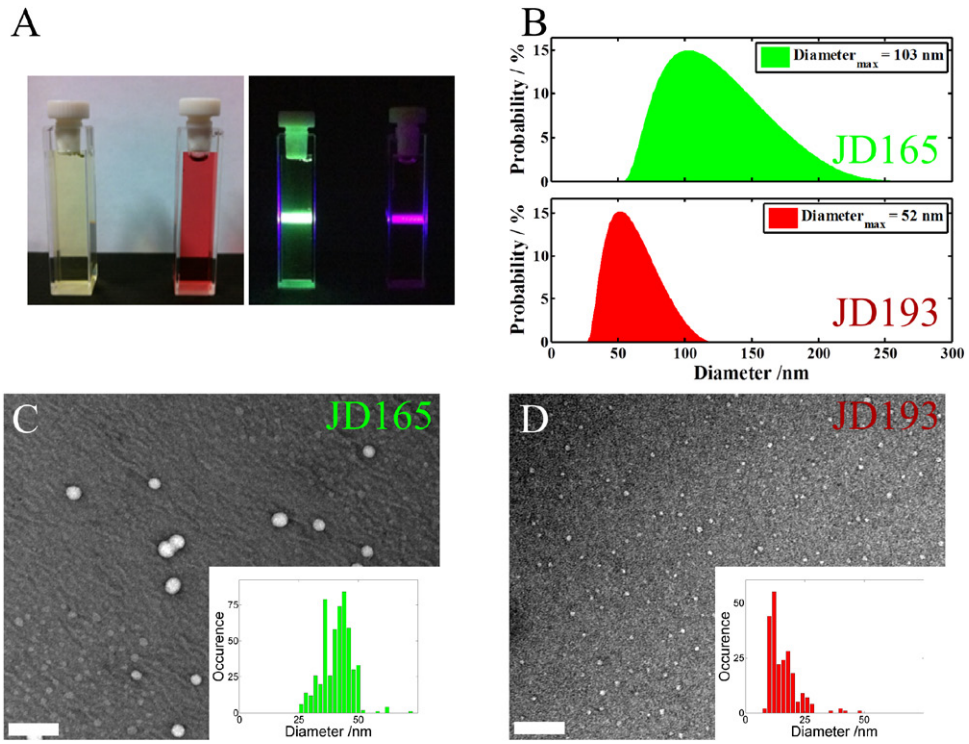

Figure 2. (A) FON suspension in water under white illumination (left) or violet (λ_{ex} ~ 405 nm) excitation (right); (B) structural characterization of JD165 and JD193 FONs using DLS. Structural characterization of JD165 (C) and JD193 (D) FONs using TEM (size distribution of JD165 and JD193 FONs presented in the inset). Scale bars: 100 nm.

Table 2. Structural characteristics of JD165 and JD193 FONs.

	D_h [a] (nm)	D_{TEM} [b] (nm)	ζ potential (mV)	N [c]
JD165 FONs	103 (102)	43	−70	29 000
JD193 FONs	52 (37)	14	−88	1100

[a] Hydrated diameter of FONs derived from DLS experiments (figure 2(B)). Values are intensity-weighted (number-weighted values are shown in parentheses).
[b] FONs diameter determined from TEM experiments (figures 2(C) and (D)).
[c] Estimated number of dyes subunits per FON based on their size.

orange emitter in organic solutions, it generates *NIR-emitting* nanoparticles. Interestingly, JD193 FONs have a fluorescence quantum yield which is only slightly reduced compared to that of JD193 dye dissolved in toluene (see table 1) although the emission is shifted by about 140 nm (which should result in a major decrease of fluorescence quantum yield unless the transition dipole significantly increases). This is clear indication that J-type aggregation effects are operative in JD193 FONs, leading to increased radiative rate compared to isolated dyes in solution.

In contrast, JD165 FONs show a less marked red-shift of its emission spectrum as compared to JD165 dye dissolved in toluene (45 nm) while its fluorescence quantum yield is markedly reduced (from 0.66 to 0.14). This marked decrease in fluorescence quantum yield might be related to both an increase in the non-radiative rate and a decrease in the radiative rate. The different organization of JD165 dye subunits within FONs as compared to that of JD193 dyes (closer to H-type aggregates) might be responsible for a lower radiative decay rate. In addition to intersystem crossing and resultant triplet state formation (already operative in solution), we believe that vibrational deactivation mediated by water molecules bound to the surface of the FONs might provide an efficient non-radiative decay channel.

2.4. Comparison of FONs and Alexa dyes

JD165 and JD193 FONs have very large Stokes' shifts compared to corresponding green- and NIR-emitting Alexa dyes (5000 and 6000 cm^{-1} respectively, table 3). The ε^{max} values for both JD165 and JD193 FONs, diluted in water up to ~nM concentration, were estimated to be orders of magnitude larger than corresponding Alexa dyes (table 3). This is mostly due to the confinement of thousands of dyes in each nanoparticle (table 2). For this reason, FONs have much brighter fluorescence than individual Alexa dyes but are significantly bulkier. Because of their smaller size and lower fluorescence quantum yield, NIR-emitting JD193 FONs are, as expected, less bright than JD165 FONs, yet they still have a brightness of almost 10^6 M^{-1} cm^{-1}, which is still over one order of magnitude larger than individual Alexa Fluor®700. Altogether, these properties make FONs ideal candidates for multicolor (SPT) experiments.

Interestingly, the overlap of the absorption spectra of both JD165 and JD193 FONs in the range 350–500 nm (figure S2(A) (stacks.iop.org/JPhysD/49/084002/mmedia)) enables their simultaneous excitation using a single excitation source. As stated before, this broad excitation range is of particular interest in multicolor imaging using three or more dyes. Indeed, despite the large width of the FON emission spectra,

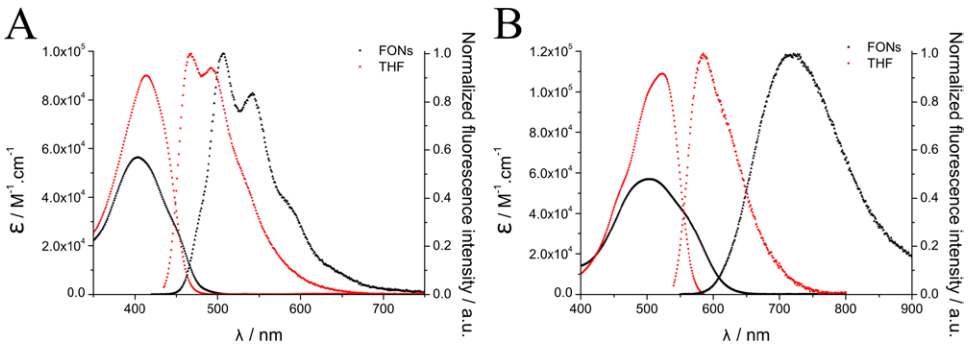

Figure 3. Comparison of absorption and emission spectra of dyes in THF (red dots) and as subunits in FONs suspension in water (black dots) for JD165 (A) and JD193 (B).

Table 3. Compared optical characteristics of JD165 and JD193 FONs to those of commercially available Alexa dyes.

	λ_{abs}^{max} (nm)	ε^{max} (M^{-1} cm^{-1})	λ_{Em}^{max} (nm)	Stokes'shift (cm^{-1})	Φ_f	$\varepsilon^{max}\Phi_f$ [a] (M^{-1} cm^{-1})	Approx. diameter (nm)
JD165 FONs	400	$1.6 \cdot 10^9$ [b]	507	5280	0.14	$2.2 \cdot 10^8$	43
Alexa Fluor®488 [1]	495	$7.3 \cdot 10^4$	519	930	0.92	$6.7 \cdot 10^4$	<2
JD193 FONs	503	$6.0 \cdot 10^7$ [b]	716	5910	0.01	$9.0 \cdot 10^5$	14
Alexa Fluor®700 [1]	702	$2.0 \cdot 10^5$	723	410	0.25	$0.5 \cdot 10^5$	<2

[a] Brightness.
[b] Value of ε^{max} for a single nanoparticle.

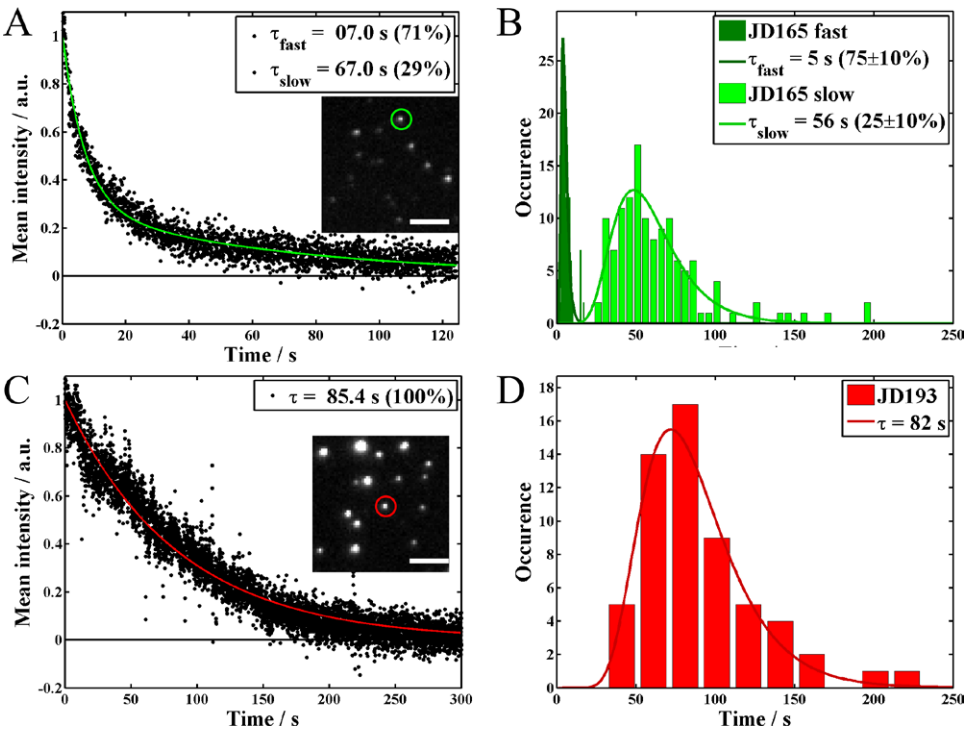

Figure 4. Photostability of the FONs (**top**: JD165; **bottom**: JD193) in water. (A) Fluorescence intensity decay of the JD165 FON highlighted in the inset (Scale bar: 5 μm). The fit of a two-component exponential decay is also presented (green line). (B) Histograms showing the distribution of decay times for both the fast and slow components ($N = 128$). The average weights of each component are also presented. The log-normal distribution that best fits the data is shown. (C) Fluorescence intensity decay of the JD193 FON highlighted in the inset (Scale bar: 5 μm). A single component exponential decay is also presented (red line). (D) Histogram showing the distribution of decay times ($N = 64$). The log-normal distribution that best fits the data is shown. A 488 nm laser with power of 1.70 kW·cm^{-2} and 0.35 kW·cm^{-2} for JD165 and JD193 FONs respectively were used in this experiment.

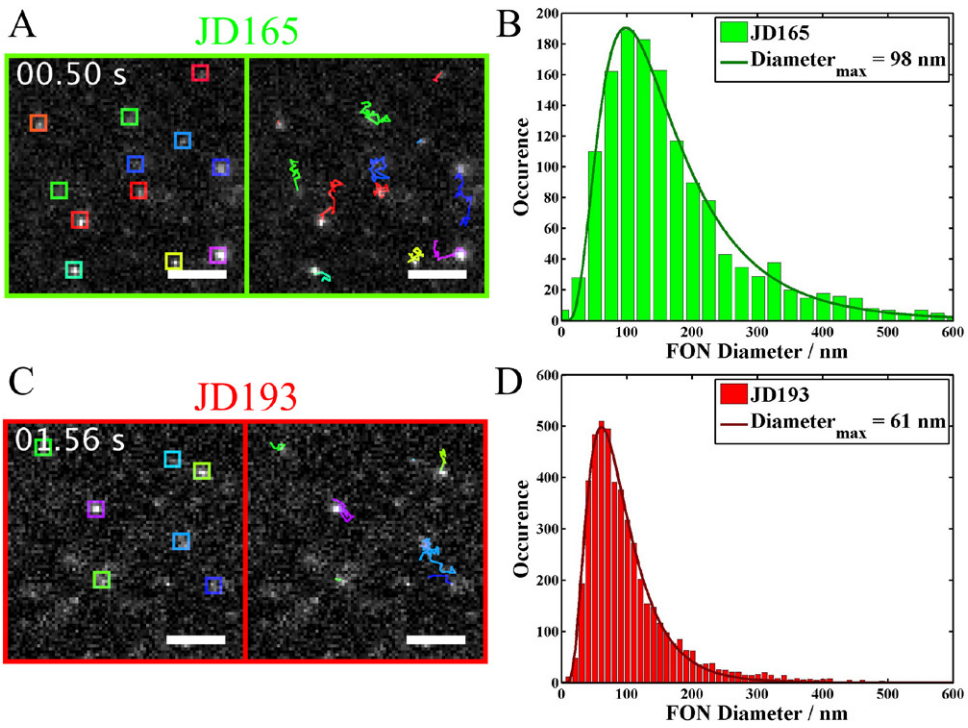

Figure 5. Single particle tracking of the FONs in water (A and C) and distribution of their hydrodynamic diameters extracted from the tracking experiments. JD165 (A) and JD193 (B) FONs were imaged freely diffusing in water (representative frames from movies S1 and S2 (stacks.iop.org/JPhysD/49/084002/mmedia) are shown in (A) and (C), respectively). The cumulative trajectories of the FONs detected in each frame (left, in colored boxes) are shown on the right sub-panels using a corresponding color code. For each single FON tracked for more than four frames, its diffusion coefficient and theoretical hydrodynamic diameter are extracted from its square displacements. Histograms of the hydrodynamic diameters are finally fitted with a log-normal distribution (D_{max}: peak value of the log-normal distribution, (B) and (D)). Scale bars: 5 μm. 488 nm laser power of 306 W·cm^{-2} was used for these experiments.

the large Stokes' shift offers the opportunity to use extra dyes emitting in different ranges such as near 400 nm, 600 nm and over 900 nm (figure 3). This provides high versatility and good compatibility with existing dyes for multicolor experiments. However, strong brightness is not sufficient for fluorescent markers to be of major interest for bioimaging purposes. Adequate photostability, enabling longtime imaging and tracking, is also a paramount prerequisite.

2.5. Single-molecule photostability study

To study whether FONs could be detected at the single molecule level, FONs were immobilized by spin-coating on a coverslip and observed through a single molecule fluorescence microscope. Water was then added before imaging. Under 488 nm laser line excitation both single JD165 and JD193 FONs could be detected for ~10–30 s at video rate. For comparison, Cy molecules, laser-irradiated under similar conditions, are photobleached in a few seconds [19]. To compare the photostability of the two types of nanoparticles, illumination intensities were chosen so that, the average initial emission photon rates were similar for both types of FONs ($P = 1.70$ kW·cm^{-2} and $P = 0.35$ kW·cm^{-2} for JD165 and JD193 FONs respectively). Although photobleaching time traces of JD193 FONs are well described by a single exponential decay, two exponential decays are required to adequately fit the intensity traces of the JD165 FONs (figures 4(A) and (C)). This might suggest that the photophysics properties of the JD193 dyes composing the smaller FONs are mainly governed by their surface chemistry while, for the larger JD165 FONs, combined effects of individual dye photophysics and multi-dye interactions within the volume of the particles should be taken into account [11]. The decay times histograms obtained from 128 JD165 and 64 JD193 single FONs are presented in figure 4. Even if both types of FONs can be detected for several seconds to minutes, the smaller JD193 FONs ($\tau_{1/2}$ ~ 82 s) are significantly more photostable compared to the larger JD165 FONs ($\tau_{1/2}$ ~ 6 s) (figures 4(B) and (D)). These values show laser power dependence and the effect of an increase in laser power on JD193 FONs photostability is shown in supplementary figure S1 (stacks.iop.org/JPhysD/49/084002/mmedia).

2.6. Single particle tracking experiments in water

As both green- and NIR-emitting FONs are bright and photostable for seconds at video rate, it is possible to track them at the single particle level in aqueous environments. Moreover, as their absorption spectra overlap (figure S2(A) (stacks.iop.org/JPhysD/49/084002/mmedia)), both green and NIR FONs can be excited with a single excitation beam (here at 488 nm) and simultaneously imaged through a dual-view system which spectrally separates the emitted fluorescent signal in a green and a NIR channels on two halves of the camera chip (see Material and methods) while the FONs are freely diffusing (figures 5 and S2(C), and movies S1–S3 (stacks.iop.org/JPhysD/49/084002/mmedia)). Note that we confirmed that no

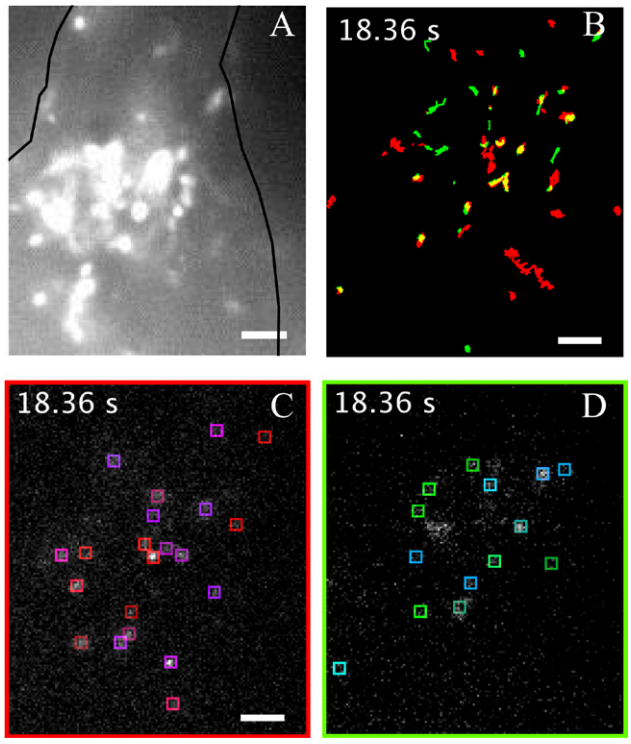

Figure 6. Single particle tracking of the FONs in live COS7 cells. COS7 cells were incubated with JD165 and JD193 FONs for 2 h, washed and imaged live under 488 nm inclined illumination. (A) Intensity average of a sub-region of a representative acquisition. The contour of the cell is drawn in black. For each channel, emitting nanoparticles are detected, fitted with a 2D-Gaussian (colored boxes in (C) and (D), NIR and green channels, resp.) and tracked between consecutive frames ((B), red and green traces for the NIR and green channels, resp.). To superpose the tracks from both channels, a simple linear transformation is applied. Analysis for one representative frame is shown (B)–(D), see movies S4 and S5 (stacks.iop.org/JPhysD/49/084002/mmedia) for the complete analysis). Scale bars: 5 μm. 488 nm laser power of 306 W·cm^{-2} was used for these experiments.

bleed through was detectable between both imaging channels (figures S1(A) and (B) (stacks.iop.org/JPhysD/49/084002/mmedia)).

From single particle trajectories lasting more than four frames, we calculated mean square displacements (MSDs). Assuming free Brownian motion (as evidenced by linear MSDs over time) and a spherical shape of the FONs, the hydrodynamic diameters of the tracked particles were then extracted (figures 5(B) and (D)). Accordingly, the peak values of the hydrodynamic diameter distributions found by SPT are consistent with hydrated diameters measured by DLS experiment (see table 2).

2.7. Application to biological samples

We then tested the suitability of these FONs for single particle experiments in a cellular environment. Fibroblast-like COS7 cells were incubated with pM concentrations of either FONs or a 4:1 mix of both types (v/v JD165 FONs: JD193 FONs) for 2 h. Cells were then washed several times in warm cell medium before being imaged under inclined [19, 20] 488 nm illumination. Even after 24 h incubation, no cytotoxicity could be observed as compared to a negative control.

FONs displayed strong fluorescence in common cell medium, retained their fluorescence in cellular vesicles, and did not present unspecific binding to the cell membrane. Strikingly, both JD165 and JD193 FONs were observed and could be simultaneously tracked in living cells (figure 6 and movies S4 and S5 (stacks.iop.org/JPhysD/49/084002/mmedia)). The relatively slow motion of the FONs and the co-localization of green and NIR FON trajectories suggest that they are naturally endocytosed in COS7 cells and that intracellular vesicles were consequently tracked. Interestingly, the presence of single-colored tracks further validates that there is no imaging channel cross-talk.

3. Conclusions

Thanks to the original molecular design of new quadrupolar dyes, we were able to obtain and characterize novel fluorescent molecular-based nanoparticles that combine high fluorescence brightness and large Stokes' shifts, and were successfully tracked as single particles in live cells. Both small NIR-emitting nanoparticles and larger green-emitting nanoparticles were obtained following simple, quick and efficient experimental protocols. The versatility of the preparation of the FONs make possible the incorporation of biofunctional groups in the nanoparticles [21] in order to combine the brightness of the FONs with targeting ability. Thanks to their broad absorption spectra, their separated emission spectra and their photostability, they were successfully imaged in a dual-color SPT proof-of-concept experiment under a monochromatic excitation wavelength. We also performed SPT in living cells using a single excitation source and a single detection camera. During imaging, no evidence of cytotoxicity of the FONs was observed. Interestingly, both types of FONs were internalized in living cells, probably in endocytic vesicles, and tracked as they were trafficking in the cytoplasm. As such, these fully organic fluorescent nanoparticles open a novel non-toxic alternative to bright quantum dots to image biological structures, including live cells, especially when multicolor SPT is at stake.

4. Materials and methods

4.1. Synthesis and characterization of the quadrupolar dyes

Commercially available reagents were used without further purification. Dry solvents were distilled from the appropriate drying reagents prior to use. All air- or water-sensitive reactions were carried out under argon. Infrared spectra were measured on a Perkin Elmer Spectrum 100 Optica. ^{1}H and ^{13}C NMR spectra were recorded on a Bruker Avance III 200 spectrometer at 200 MHz and 50 MHz respectively or Bruker Avance I 300 spectrometer at 300 MHz and 75 MHz respectively. ^{1}H chemical shifts (δ) are reported in ppm, coupling constants (J) are given in Hertz, ^{13}C chemical shifts are given relative to the central peak of CD_2Cl_2 at 54.0 ppm.

High-resolution mass spectra measurements were performed at CESAMO (Bordeaux, France). Melting points were determined on Mettler Toledo DSC 1.

4.2. Photophysical studies

All photophysical properties were analyzed with freshly prepared air equilibrated solutions at room temperature (293 K). UV/Vis absorption spectra were recorded using a Jasco V-570 spectrophotometer. Steady-state fluorescence measurements were performed on dilute solutions (optical density <0.1) contained in standard 1 cm quartz cuvettes using a Horiba (FluoroLog or FluoroMax) spectrometer in photon-counting mode. Fully corrected emission spectra were obtained for each compound at $\lambda_{ex} = \lambda_{abs}^{max}$ with an optical density at $\lambda_{ex} \leqslant 0.1$ to minimize internal absorption. Fluorescence quantum yields were measured according to literature procedures [22, 23] using fluorescein in 0.1 M NaOH ($\Phi_f = 0.9$) or cresyl violet in MeOH ($\Phi_f = 0.54$).

The extinction coefficients of JD165 and JD193 dyes in water were calculated using the concentration of chromophores in water. These concentrations were 10 μM for JD165 and 5 μM for JD193.

4.3. Preparation of the FONs

Nanoparticles of either JD165 or JD193 quadrupoles were prepared using the reprecipitation method. The FONs were obtained by instantaneous addition of a solution of the corresponding chromophores in THF (1 mM for JD165 or 0.5 mM for JD193) in distilled water under sonication at 10 W for 3 min (using a VibraCell 1300 W sonicator with a probe of 6 mm of diameter). The total amount of THF in the suspension of FONs is set to be lower than 1% for lowering any toxic effect due to the presence of the organic solvent. After the addition was completed, the solution quickly evolved from colorless to yellow (JD165 FONs) or reddish (JD193 FONs).

4.4. Characterization of the FONs

TEM imaging was carried out using a HITACHI H7650. Copper grids coated with a carbon membrane were pretreated using the Glow discharge technique to yield to positively charged grids thus helping the interaction between the FONs and the grid. One droplet of the aqueous FONs suspension was deposited on the grid followed, once the excess of liquid was drown-off with paper, by a staining procedure using uranyl acetate. DLS experiments were performed using a SZ-100Z Horiba instrument operating at 173°. Hydrodynamic diameters (D_h) were calculated from diffusion coefficients using the Stokes-Einstein equation. All correlogram analyses were performed using the software supplied by the manufacturer and are represented in scattering light intensity. Zeta-potential analysis was performed with the SZ-100Z Horiba instrument. Several measurements were realized for each sample according to a predefined operating procedure.

The brightness of each type of FONs in water was estimated using the concentrations (0.3 nM for JD165 FONs and 4.5 nM for JD193 FONs) determined by the average dye subunit number per FONs based on their D_{TEM} size (see table 3).

4.5. Fluorescence imaging setup

All widefield fluorescence images were acquired using a custom-made inverted microscope [19] with a 60 × oil-immersion objective of 1.45 numerical aperture (Plan Apo TIRF, Nikon or PlanApo TIRFM, Olympus), and a fast EMCCD camera (ProEM 512B, Princeton Instruments or QuantEM:512SC, Photometrics). Illumination at 488 nm was obtained with a 150 mW OBIS 488LX laser.

4.5.1. Photobleaching experiments. Time series of immobilized FONs were acquired independently for each type of FONs. Imaging time was set to 50 ms. For these experiments, a dichroic mirror FF495-Di03 (Semrock) was used in combination with the emission filter HQ525/50m (Chroma) for the JD165 FONs and BLP01-635R (Semrock) for JD193 FONs. To adequately compare the photostability of the two types of FONs presented here, different laser powers were used to illuminate the sample in order to obtain in average, the same initial emission photon rates for the two nanoparticle types.

4.5.2. Single-particle tracking experiments in water. Movies of freely diffusing FONs in water were recorded at fast acquisition speed. Exposure time of the camera was set to 10 ms. Images were independently acquired for both types of FONs. For the single-particle experiments, a dichroic mirror FF495-Di03 (Semrock) was used in combination with the emission filter HQ525/50m (Chroma) for the JD165 FONs, or BLP01-635R (Semrock) for JD193 FONs.

4.5.3. Dual-color imaging. For the dual-color imaging experiments, emitted light was separated from the 488 nm illumination thanks to a dichroic mirror (FF495-Di03, Semrock). Then, the fluorescence signal was spectrally split in two by a dichroic beam-splitter (FF655-Di01, Semrock) placed at the Fourier plane of a relaying 4f optical system. Each channel was further filtered (HQ525/50m, Chroma for the JD165 FONs, and FF01-776/LP, Semrock, for the JD193 FONs) and projected on one half of the EMCCD camera. To image freely diffusing FONs in water, the exposure time was set to 10 ms. When FONs were imaged in a cellular environment, the exposure time was 62.5 ms. The power of the 488 nm laser was adjusted so that the power density of the illumination at the sample reached 1 kW cm^{-2} for these experiments.

4.6. Photobleaching analysis

To analyze movies of the immobilized photobleaching FONs, circular regions of interest (ROIs) containing single FONs were delineated using a home-build Matlab routine. A nearby region defining the local background was also associated to each selected ROI that contained a nanoparticle. Traces of the

integrated intensity inside each ROI, from which was subtracted the total intensity in the corresponding background region, were obtained and fitted with a linear combination of one or two exponential decays.

4.7. SPT analysis

Similarly to previously described experiments [19, 24], intensity maxima were detected after frequency filtering, and separated point-spread functions were fitted with 2D-Gaussians (thanks to indifferently a Matlab routine or the PeakFit software) [25, 26]. Nearest neighbor localizations in consecutive frames were joined in trajectories if they were spatially closer than 200–300 nm. In the case of slow moving particles, in COS7 cells, to allow for some inefficiency in the localization fitting step, eligible nearest neighbors were searched for in up to five previous frames. Finally, in case of merging or splitting of trajectories, the longest trajectories were concatenated, and the smallest ones, ended at the meeting point. In all cases, computed trajectories were qualitatively confronted to the original acquisition (e.g. movies S1, S2, S4 and S5 (stacks.iop.org/JPhysD/49/084002/mmedia)).

4.8. Cell culture

Fibroblast-like COS-7 cells were grown in Dulbecco's Modified Eagle Medium without phenol-red (PAN Biotech, P04-01515) supplemented with 10% v/v foetal calf serum (FCS—Dominique Dutscher, 500105), 1% v/v penicillin/streptomycin (Dominique Dutscher, P06-07100) in 25 ml flasks (Falcon, 353082) at 37 °C, 5% CO_2. They were kept below 90% confluency, at which cells were washed in sterile filtered PBS (PAN Biotech, P04-36500), detached in a small volume of trypsin (PAN Biotech, P10-021100), washed in full warm medium and split 1/10 in a new flask. For imaging, 90% confluent cells were similarly detached with trypsin and diluted 1/10 in full warm medium. Eighteen mm-diameter round #1.5 coverslips (Thermo Scientific, DV40008) were placed in a 12-well plate (Cellstar, 665180); each coverslip was incubated in 500 μl spectrograd-rated ethanol (Fluka, 02850-1L) for $>$10 min, thoroughly washed twice in PBS, and resuspended in 2 mL of full warm medium. Volumes of 100 μl of diluted cells were then dropped onto each coverslip. Cells were carefully homogenized by tilting the 12-well plate, and left at 37 °C, 5% CO_2 overnight. Cells were then washed in warm cell medium and incubated for 2 h with 40 μl of 0.3 nM JD165 FONs and 10 μl of 4.5 nM JD193 FONs in 1 ml cell medium. Before imaging, cells were thoroughly washed twice with warm FCS-free cell medium.

Acknowledgments

We acknowledge financial support from Bordeaux Idex project (ANR-10-IDEX-03-02, 'Investments for the future'), the Conseil Régional d'Aquitaine (Chair of Excellence to MBD, fellowship to JD, grant 2011-1603009 to LC), France-BioImaging infrastructure supported by the French National Research Agency (ANR-10-INSB-04, 'Investments for the future'), the Fonds Recherche du Québec—Nature et Technologies (fellowship to AGG), the CNRS, the French Ministry of Education and Research, and the Agence Nationale de la Recherche. TEM microscopy was done in the Bordeaux Imaging Center (UMS 3420 CNRS—University of Bordeaux/Inserm US4). The help of Sabrina Lacomme is acknowledged.

References

[1] Spence M T Z and Johnson I D 2010 *The Molecular Probes Handbook: A Guide to Fluorescent Probes and Labeling Technologies* 11th edn (Carlsbad, CA: Life Technologies) p 1060
[2] ATTO-TEC 2009 *Fluorescent Labels and Dyes* (Siegen: ATTO-TEC) pp 1–99
[3] Lippincott-Schwartz J and Patterson G H 2003 Development and use of fluorescent protein markers in living cells *Science* **300** 87–91
[4] Shaner N C, Steinbach P A and Tsien R Y 2005 A guide to choosing fluorescent proteins *Nat. Methods* **2** 905–9
[5] Krishna T R, Parent M, Werts M H V, Moreaux L, Gmouh S, Charpak S, Caminade A-M, Majoral J-P and Blanchard-Desce M 2006 Water-soluble dendrimeric two-photon tracers for *in vivo* imaging *Angew. Chem., Int. Ed. Engl.* **45** 4645–8
[6] Fery-Forgues S 2013 Fluorescent organic nanocrystals and non-doped nanoparticles for biological applications *Nanoscale* **5** 8428–42
[7] Horn D and Rieger J 2001 Organic nanoparticles in the aqueous phase—theory, experiment and use *Angew. Chem., Int. Ed. Engl.* **40** 4330–61
[8] Masuhara H, Nakanishi H and Sasaki K 2003 *Single Organic Nanoparticles* (New York: Springer) p 402
[9] Groc L, Lafourcade M, Heine M, Renner M, Racine V, Sibarita J-B, Lounis B, Choquet D and Cognet L 2007 Surface trafficking of neurotransmitter receptor: comparison between single-molecule/quantum dot strategies *J. Neurosci.* **27** 12433–7
[10] Pinaud F, Clarke S, Sittner A and Dahan M 2010 Probing cellular events, one quantum dot at a time *Nat. Methods* **7** 275–85
[11] Genin E, Gao Z, Varela J A, Daniel J, Bsaibess T, Gosse I, Groc L, Cognet L and Blanchard-Desce M 2014 'Hyper-bright' near-infrared emitting fluorescent organic nanoparticles for single particle tracking *Adv. Mater.* **26** 2258–61
[12] Mongin O, Porres L, Chariot M, Katan C and Blanchard-Desce M 2007 Synthesis, fluorescence, and two-photon absorption of a series of elongated rodlike and banana-shaped quadrupolar fluorophores: a comprehensive study of structure-property relationships *Chem. Eur. J.* **13** 1481–98
[13] Palayangoda S S, Cai X, Adhikari R M and Neckers D C 2008 Carbazole-based donor-acceptor compounds: highly fluorescent organic nanoparticles *Org. Lett.* **10** 281–4
[14] Katan C, Tretiak S, Werts M H V, Bain A J, Marsh R J, Leonczek N, Nicolaou N, Badaeva E, Mongin O and Blanchard-Desce M 2007 Two-photon transitions in quadrupolar and branched chromophores: experiment and theory *J. Phys. Chem.* B **111** 9468–83
[15] Terenziani F, Painelli A, Katan C, Charlot M and Blanchard-Desce M 2006 Charge instability in quadrupolar chromophores: symmetry breaking and solvatochromism *J. Am. Chem. Soc.* **128** 15742–55
[16] Amthor S, Lambert C, Dümmler S, Fischer I and Schelter J 2006 Excited mixed-valence states of symmetrical donor–acceptor–donor π systems *J. Phys. Chem.* A **110** 5204–14

[17] Strickler S J and Berg R A 1962 Relation between absorption intensity and fluorescence lifetime of molecules *J. Chem. Phys.* **37** 814–22
[18] Kasha M, Rawls H R and El-Bayoumi M A 1965 Exciton model in molecular spectroscopy *Pure Appl. Chem.* **11** 371–92
[19] Winckler P, Lartigue L, Giannone G, De Giorgi F, Ichas F, Sibarita J-B, Lounis B and Cognet L 2013 Identification and super-resolution imaging of ligand-activated receptor dimers in live cells *Sci. Rep.* **3** 2387
[20] Tokunaga M, Imamoto N and Sakata-Sogawa K 2008 Highly inclined thin illumination enables clear single-molecule imaging in cells *Nat. Methods* **5** 159–61
[21] Li K, Jiang Y, Ding D, Zhang X, Liu Y, Hua J, Feng S-S and Liu B 2011 Folic acid-functionalized two-photon absorbing nanoparticles for targeted MCF-7 cancer cell imaging *Chem. Commun.* **47** 7323–5
[22] Eaton D F 1988 Reference materials for fluorescence measurement *Pure Appl. Chem.* **60** 1107–14
[23] Crosby G A and Demas J N 1971 Measurement of photoluminescence quantum yields: review *J. Phys. Chem.* **75** 991–1024
[24] Godin A G, Lounis B and Cognet L 2014 Super-resolution microscopy approaches for live cell imaging *Biophys. J.* **107** 1777–84
[25] Sage D, Kirshner H, Pengo T, Stuurman N, Min J, Manley S and Unser M 2015 Quantitative evaluation of software packages for single-molecule localization microscopy *Nat. Methods* **12** 717–24
[26] www.sussex.ac.uk/gdsc/intranet/microscopy/imagej/smlm_plugins